Electrochemical Reactions Between Perovskite-Type LaCoO$_3$ and Lithium

D.W. ZHANG, S. XIE & C.H. CHEN*

Department of Materials Science and Engineering, University of Science and Technology of China, Anhui Hefei 230026, P.R. China

Abstract. The perovskite-type composite metal oxide LaCoO$_3$ was firstly used as an electrode material in rechargeable lithium cells. X-ray diffraction (XRD), scanning electron microscopy (SEM) and extended X-ray absorption fine structure (EXAFS) were employed to analyze the structures of synthesized and discharged LaCoO$_3$ samples. Cyclic voltammetry and galvanostatic cell cycling were used to characterize the electrochemical performance of LaCoO$_3$/Li cells. A stable reversible capacity from 110 to 130 mAh/g during up to 50 cycles can be achieved. Based on the analyses of ex-situ XRD and EXAFS of the lithiated/delithiated LaCoO$_3$ electrode, a three-step electrochemical reaction mechanism was proposed.

Keywords: perovskite, lanthanum cobaltite, lithium ion battery, electrode, EXAFS

1. Introduction

During the last two decades, a number of electrode materials with different mechanisms of lithium insertion and extraction have been developed for lithium-ion batteries. In these materials, graphite is currently used as the state-of-the-art anode material in commercial lithium-ion batteries. Their reaction mechanism is reversible insertion and extraction of lithium in a host structure. Nevertheless, in order to find more advanced electrode materials, many research groups are still searching for alternative anode materials systems that can ensure the cells maintain their high capacity and mechanical integrity over long time charge-discharge cycling.

In recent years, there has been an increasing interest in the use of metal oxides as the anode electrode for lithium ion batteries. Idota et al. [1] reported a new high capacity anode material that consists of tin-based amorphous oxides. The lithium reaction mechanism relies on the formation of Li–Sn alloys. Similarly, Li et al. [2] studied a high capacity anode material SnO$_2$ with nanostructure. This nanostructured SnO$_2$-based

electrode has extraordinary rate capabilities and can deliver very high capacities (e.g., 700 mAh/g at 8C rate) over as many as 1400 cycles. The lithium reaction mechanism also relies on the formation of Li–Sn alloys.

Poizot et al. [3] reported that an electrode made of nanoparticles of transition metal oxides (MO, where M is Co, Ni, Cu or Fe) demonstrates a good electrochemical reversible capacity. Wang et al. [4, 5] also investigated a series of cobalt oxides as anode materials. All these cobalt oxides demonstrated fairly good electrochemical properties as lithium storage materials in Li-ion batteries. A displacement mechanism based on the formation and decomposition of Li$_2$O, with concurrent reduction and oxidation of metal nanoparticles was proposed. It is different from the conventional intercalation mechanism as for LiCoO$_2$ and graphite, and may lead to the discovery of new electrodes.

Up to now, most of the studies on this new type of electrode material have been concentrated on mono-metal oxides although a few binary metal oxides such as CoSnO$_3$ [6], NiCo$_2$O$_4$ [7] and CaSnO$_3$ [8] were also investigated. In this paper we report another binary metal oxide, perovskite-type LaCoO$_3$, as a possible anode material for lithium-ion batteries. Because LaCoO$_3$ and its Sr-doped derivatives are very good mixed conductors of electrons and oxide ions [9, 10],

*To whom all correspondence should be addressed. E-mail: cchchen@ustc.edu.cn

it is interesting to study the mixed conduction of electron and lithium ion in this material. Furthermore, as an anode material in a lithium cell, the electrochemical reaction pathways during charge-discharge process must be clarified.

2. Experimental

Lanthanum cobaltite $LaCoO_3$ powder was synthesized by the pyrolysis of a polymerizable complex (PC) [11] based on the Pechini-type reaction route. Starting material for the PC method was lanthanum oxide (99.99%), cobalt nitrate (analytically pure), citric acid (analytically pure) and ethylene glycol (analytically pure). $La(NO_3)_3$ solution was obtained by dissolving La_2O_3 in HNO_3 solution. Citric acid (CA) was dissolved in deionized water then stoichiometric $La(NO_3)_3$ solution and $Co(NO_3)_2$ were added into it. The mixture was magnetically stirred at 60°C for 2 h in order to obtain in the solution stable metal–CA complexes. When a clear pink solution was thus obtained, ethylene glycol (EG) was added to this solution. The solution thus obtained was continuously stirred with a magnetic stirrer at 90°C for 10 h to obtain a viscous mass. Then the polymeric resin was heated at 400°C to decompose the polymer. The product after the decomposition was slightly ground into powder that was then calcined at 900°C for 10 h. Thus obtained powder was pressed into pellets and sintered at 1100°C for 10 h. Then the sintered pellets were ground into fine powder for making electrode.

The compositions of the products obtained at different sintering temperature were characterized by X-ray diffraction (XRD) (Philips X'Pert PRO SUPER, CuKα radiation). The microstructure of the materials was evaluated by scanning electron microscopy (SEM).

The electrochemical performance of $LaCoO_3$ as an electrode was measured using two-electrode coin cells (CR2032) of the Li|1M $LiPF_6$(EC:DEC = 1:1)|$LaCoO_3$. The $LaCoO_3$ electrode laminate was prepared as 14 mm diameter pellets by casting a slurry consisting of 84 wt% active oxide, 8 wt% poly(vinylidene fluoride) (PVDF) binder, and 8 wt% carbon black onto a copper foil. Celgard 2400 microporous polypropylene membrane was used as separator. These cells were cycled galvanostatically between 0 and 3 V at room temperature on a multi-channel battery test system (NEWARE BTS-610) to analyze the electrochemical response. Cyclic voltammetry (CV) was also performed to determine the characteristics of the lithium reaction with the $LaCoO_3$ electrodes.

The evolution of the crystalline structure of the electrode material during cycling was determined by means of an ex-situ X-ray diffraction (XRD). The assembled coin cells were firstly discharged to different stages on the battery test system and then were opened in the glove box. The partially lithiated electrode pellet was washed with diethyl carbonate (DEC) and then was sealed in thin, transparent polyethylene bags respectively after drying.

Extended X-ray absorption fine structure (EXAFS) was adopted to study the local structure of the final lithiated products. The EXAFS data were collected from the XAFS station of National Synchrotron Radiation Laboratory. $LaCoO_3$ electrode was discharged to 0 V and treated with the same way as ex-situ XRD. Then the Co K-edge spectra and La L_{III}-edge spectra of the final lithiated products were respectively obtained on the XAFS station. Co K-edge spectra of $LaCoO_3$ pristine powders and La L_{III}-edge spectra of La_2O_3 pristine powders were also obtained to compare with the spectra of the final lithiated products.

To investigate more details of the lithiated and delithiated structural and morphological changes, we also studied $LaCoO_3$-based electrodes after full lithiated by means of a field emission scanning electron microscope. After fully discharged in the first cycle, the coin cell was disassembled and the working $LaCoO_3$ electrode was washed with diethyl carbonate (DEC) in the glove box. Then the electrode was used for SEM examination.

3. Results and Discussion

3.1. Structural Analyses of LaCoO₃ Powders

Figure 1 shows the XRD patterns of lanthanum cobalt oxide sintered at 900 and 1100°C. A single perovskite-type hexagonal phase of $LaCoO_3$ with a rhomb-centered lattice [12] is obtained already at 900°C, but further sintering at 1100°C leads to a more crystallized structure. In fact, this hexagonal phase can be regarded as a rhombohedral structure with a small distortion. For the 1100°C-sintered powder, the lattice parameters derived from a Rietveld refinement are $a = 5.3742 \pm 0.0002$ Å, $\alpha = 60.82 \pm 0.01°$. The average crystallite size of this powder is calculated to
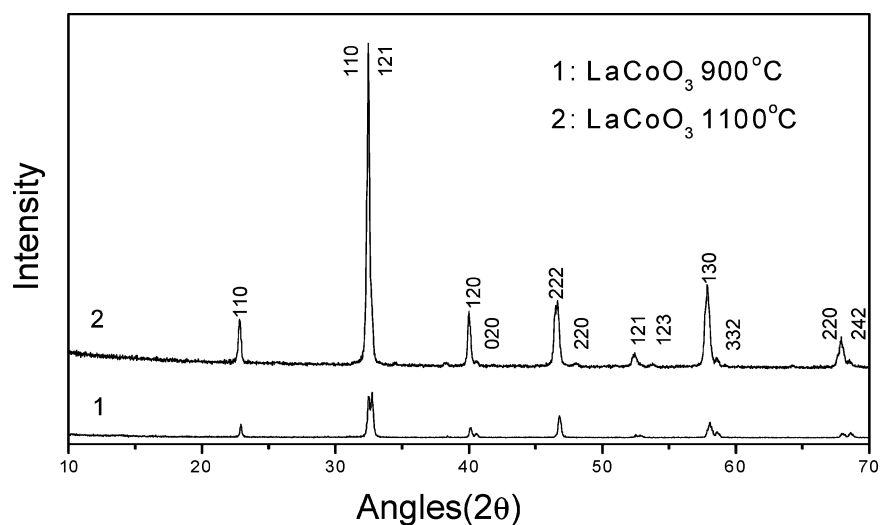
Fig. 1. XRD patterns of LaCoO₃ powders sintered at 900 and 1100°C in air.

be about 40 nm by the Scherrer equation [13]. Due probably to the differences in the extent of crystal distortion and in the preferential orientations of the lattice planes resulted from different sintering temperatures, the relative intensities of the diffraction lines for the 900°C-sintered powder (pattern 1 in Fig. 1) show slight differences compared with that of the 1100°C-sintered powder (pattern 2 in Fig. 1). Nevertheless, the average crystallite size of the 900°C-sintered powder is smaller, as evidenced by its broader diffraction peaks.

Figure 2 shows the SEM images of LaCoO₃ sintered at 900 and 1100°C. Obviously, the particle size increases from about 0.6 μm at 900°C to 1.2 μm at 1100°C. Comparing the smoothness of the particle surface, one can see the increased crystallinity of the 1100°C-sintered powder.
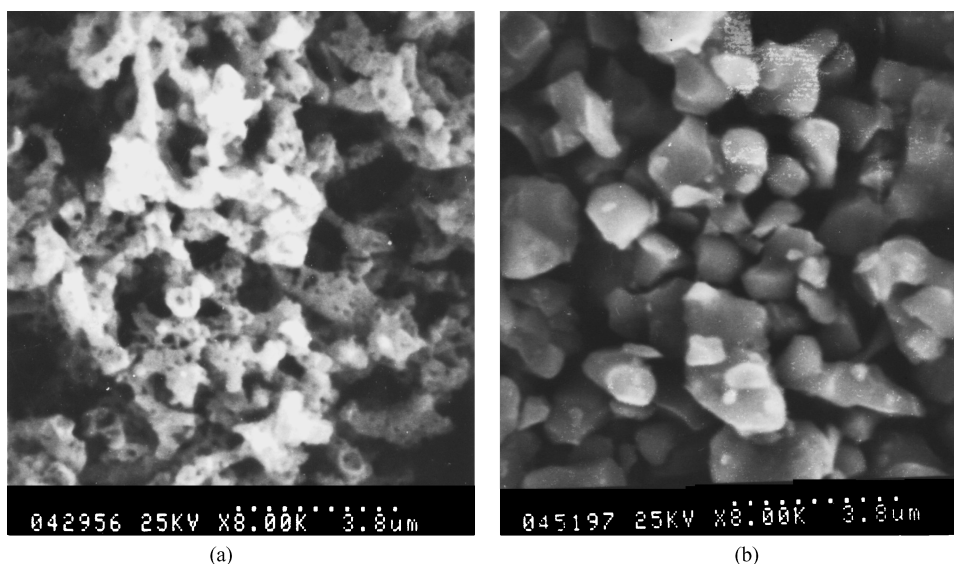

Fig. 2. SEM images of LaCoO₃ powders sintered at 900 and 1100°C in air. (a) LaCoO₃ powders sintered at 900°C with the magnification of 8000. (b) LaCoO₃ powders sintered at 1100°C with the magnification of 8000.
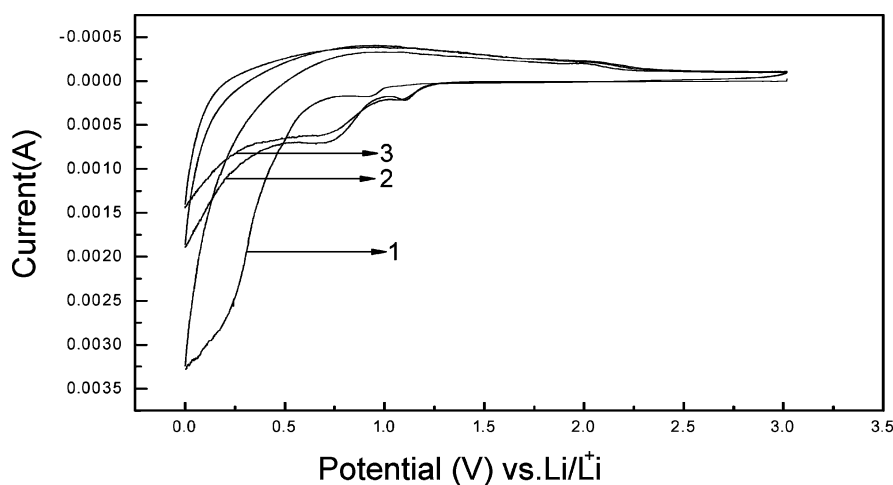
Fig. 3. Cyclic voltammograms of LaCoO$_3$ electrodes in Li-ion cells. The scanning rate is 0.2 mV/s. The voltage ranges from 3 V to 0 V.

3.2. Electrochemical Properties of LaCoO$_3$ as Anode Material

The cyclic voltammograms of a LaCoO$_3$/Li cell are presented in Fig. 3. In the first discharge process when lithium is inserted two reduction steps in the potential range of 0–3 V versus Li/Li$^+$ are found, the first with a peak potential at 0.93 V and the second with the onset potential at 0.7 V. Also, two broad oxidation peaks around 1.0 V and 2.0 V can be discerned when lithium is extracted in the first charge process. In the following cycles there exist two reduction peaks in 1.1 V, 0.7 V during the lithium insertion process, and again two broad oxidation peaks at 1.0 V and 2.0 V during the lithium extraction process.

The small reduction peak at 0.93 V in the first discharge process should be related to the formation of the SEI film (solid electrolyte interface) on the surface of the electrode because a passivation film is inevitably formed due to the decomposition of the organic electrolyte [5]. The huge reduction step with the onset potential at 0.7 V should be related to the reaction of LaCoO$_3$ with Li. The two reduction peaks at 1.1 V and 0.7 V in the subsequent cycles indicate the reduction process must proceed in two consecutive steps during lithium insertion.

The voltage profile of a LaCoO$_3$/Li cell in the discharge curves (Fig. 4) shows the electrochemical charge-discharge behavior between 0–3 V. It is clear that an irreversible reaction occurs during the first discharge process. When discharged, the potential of the

LaCoO$_3$ electrode rapidly drops to less than 1.0 V and then continuously decreases down to the cut-off voltage of 0 V. The LaCoO$_3$ (sintered at 1100°C) electrode has a large irreversible capacity during the first cycle, which is similar to the behavior of CoO electrode [4]. After the first cycle the LaCoO$_3$ (sintered at 1100°C) electrode sustains stable cycleability. It has a reversible capacity of 110 mAh/g after 25 cycles (shown in Fig. 5). Similarly, a large irreversible capacity is also present for the LaCoO$_3$ electrode with the 900°C-sintered powders, but the reversible capacity is 130 mAh/g.

3.3. Reaction Mechanism of LaCoO$_3$ with Lithium in Li-ion Cells

Based on the cyclic voltammograms (Fig. 3) and the voltage profiles (Fig. 4) of the LaCoO$_3$/Li cell, in the first discharge process LaCoO$_3$ begins to react with lithium at about 0.7 V. The specific capacity of the 0.7 V plateau (Fig. 4) is about 110 mAh/g, corresponding to the consumption of one mole of lithium (1 Li) per mole of LaCoO$_3$. About two moles of lithium (2 Li) (corresponding to about 220 mAh/g capacity) are consumed in the rest of reduction reaction. Thus, overall three moles of lithium (3 Li) are inserted into one mole of LaCoO$_3$ in the first discharge process. In the subsequent cycles, only about 110 mAh/g is reversible. This suggests that the reduction of LaCoO$_3$ with Li is only partially reversible. Ex-situ X-ray diffraction patterns
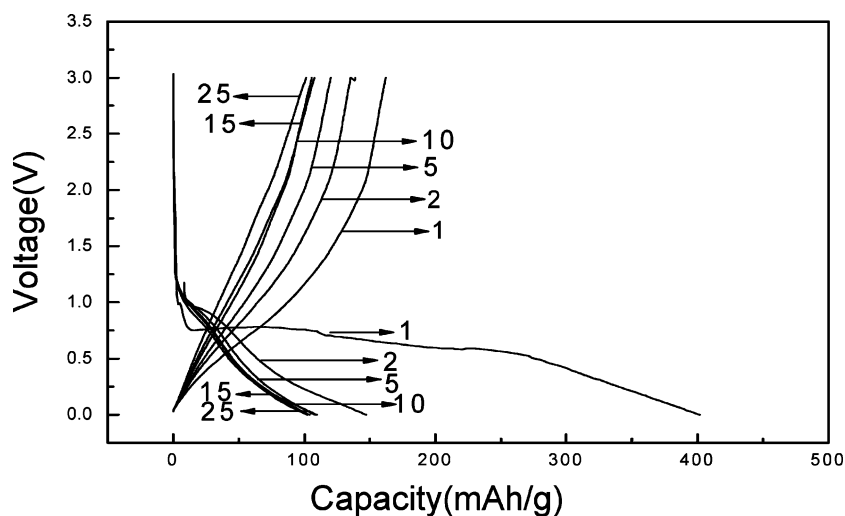
Fig. 4. The charge-discharge curves of the electrode LaCoO$_3$/Li cell. The charge-discharge was operated in the voltage range between 3.0 and 0 V at the current density of 0.1 mA/cm^2, the cycle numbers are indicated. The LaCoO$_3$ was sintered at 1100°C.
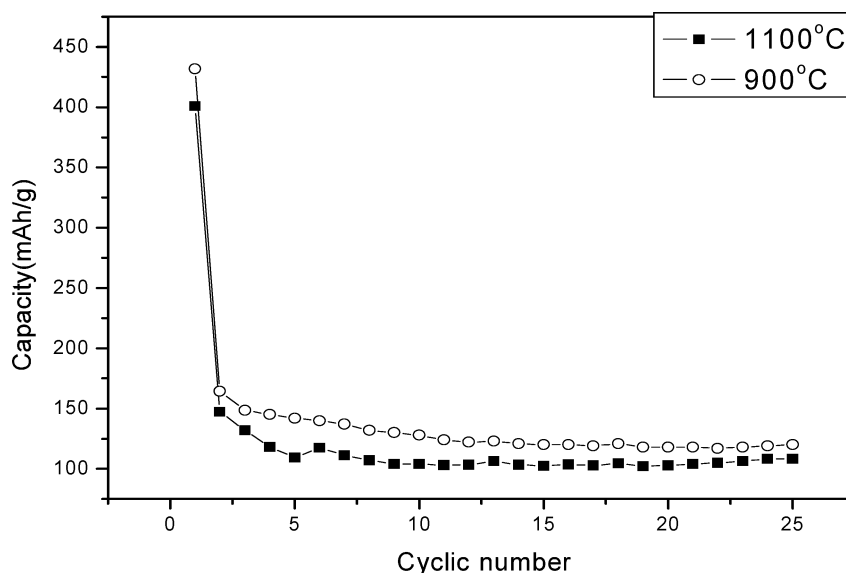

Fig. 5. Specific capacity as a function of cycle number for LaCoO$_3$(1100°C)/Li cells and LaCoO$_3$(900°C)/Li cells. The charge-discharge was operated in the voltage range between 3.0 and 0 V at the current density of 0.1 mA/cm^2, the cycle numbers are indicated.

of the LaCoO$_3$ electrodes (with the 1100°C-sintered powder) after different extents of lithiation were acquired and are shown in Fig. 6, in which the main diffraction peaks from the copper substrate can be identified. Besides, two weak and broad peaks at about 32 and 47°, which correspond to the two strongest peaks of LaCoO$_3$, can be discerned from these patterns. This

result demonstrates that although a very small amount of LaCoO$_3$ is still present after lithiation, most of the LaCoO$_3$ loses crystallinity upon cycling and the electrochemically formed lithiated products are in the form of nano-particles or amorphous structure.

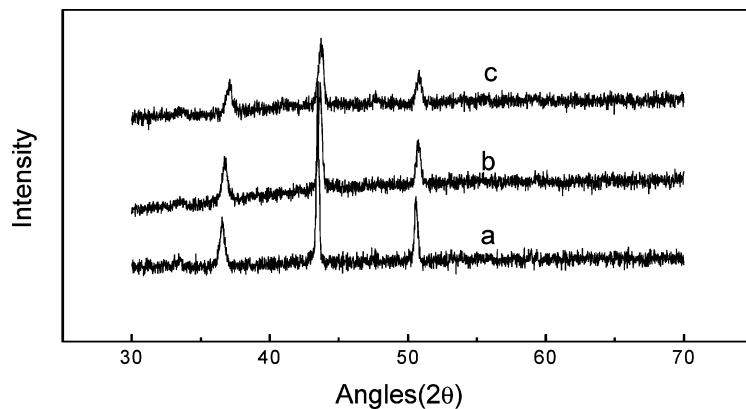The results of EXAFS analysis of the final lithiated products and LaCoO$_3$ pristine powder are shown

Fig. 6. Ex-situ X-ray diffraction of $LaCoO_3$ electrode in different lithiated/delithiated stages in the first cycle. (a) discharged to 0.3 V (b) discharged to 0 V (c) charged to 2.0 V. The $LaCoO_3$ was sintered at $1100°C$.
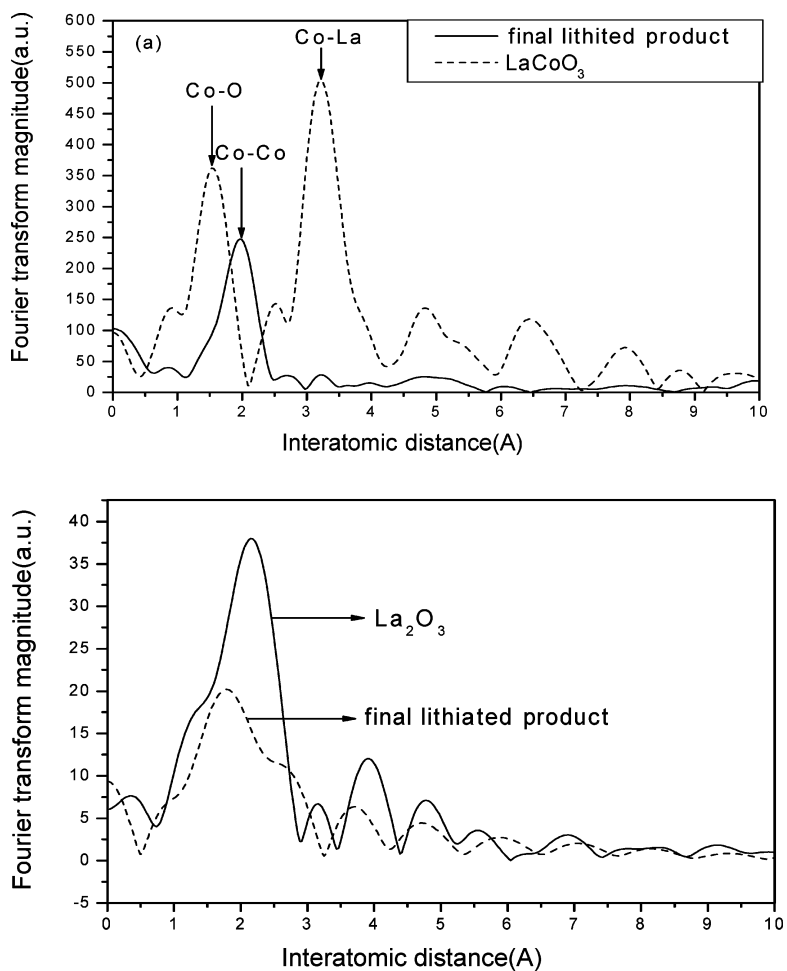

Fig. 7. EXAFS after Fourier transforms for final lithiated $LaCoO_3$ electrode, $LaCoO_3$ pristine powder and La_2O_3 pristine powder. (a) Co K-edge spectra for final lithiated $LaCoO_3$ electrode and $LaCoO_3$ pristine powder. (b) La L_{III}-edge spectra for final lithiated $LaCoO_3$ electrode and La_2O_3 pristine powder.

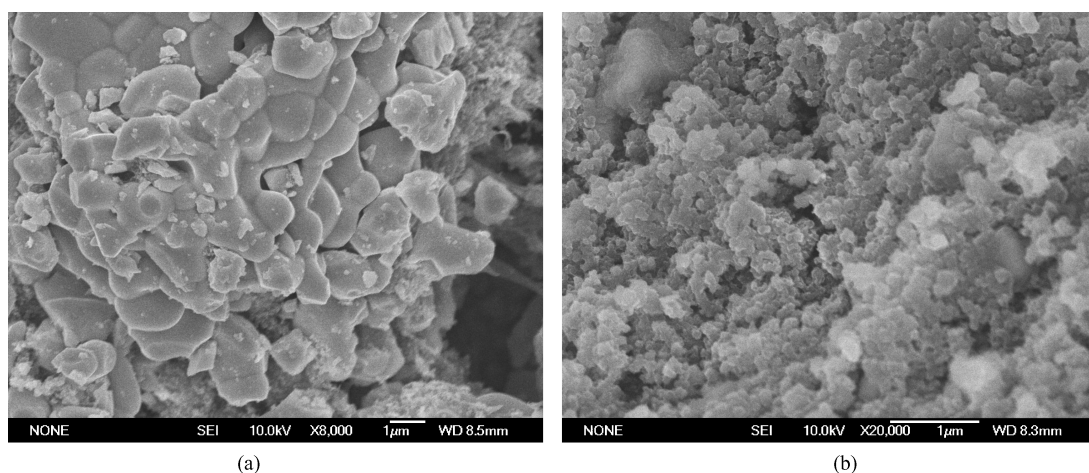(a)   (b)

Fig. 8. The typical SEM mircographs of the original LaCoO$_3$ (sintered at 1100°C) powder and LaCoO$_3$(1100°C) electrode after full discharged. (a) original LaCoO$_3$ powder sintered at 1100°C with the magnification of 8000. (b) LaCoO$_3$ (1100°C) electrode with the magnification of 20000.

in Fig. 7. Figure 7(a) shows the Co-edge spectra for the final lithiated products and LaCoO$_3$ pristine powder. It can be seen that in LaCoO$_3$ pristine powder there are Co—O bond and Co—La bond, but in the final lithiated products only Co—Co bond exists. This result shows that when LaCoO$_3$ electrode is discharged to 0 V, the product is metallic Co rather than cobalt oxide. On the other hand, the possibility of forming metallic La should be clarified. Figure 7(b) shows the La-edge spectra for the final lithiated products and La$_2$O$_3$ pristine powder. Obviously, only La—O bond rather than La—La bond exists in the reduction product. It is noticed that the position of the main peak shifts a little from that of the La$_2$O$_3$ sample. Such a shift can be attributed to the differences in measurement conditions and the degree of disorder of the samples. Thus, the product is La$_2$O$_3$ not metallic La.

Figure 8(a) shows the morphology of the initial electrode that indicates that initial LaCoO$_3$ powders consist of well-crystallized particles having dimensions of about 1 μm. When LaCoO$_3$ is fully reduced by lithium, the image (Fig. 8(b)) shows a complete disintegration of the starting 1 μm particles into 50–100 nm nanoparticles. This discharged process can be described as an electrochemical milling process, which makes the whole morphology of the electrode become amorphous. Thus, the fully reduced product must form a nano-particle matrix.

Poizot et al. [3] proposed the reaction mechanism of cobalt oxide with lithium in Li-ion cells as a displacive

redox reaction:

$$CoO + 2Li \longleftrightarrow Co + Li_2O$$
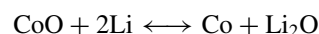
In this reversible reaction the reaction of Li$_2$O with Co to form CoO and Li is thermodynamically impossible because Li$_2$O is electrochemically inactive. The extraction of Li from Li$_2$O is thermodynamically impossible. However, they argued that the chemical and physical phenomena are strongly affected when dealing with nano-sized materials. Since the electrochemically formed Li$_2$O and Co are nanoparticles in nature, the electrochemically driven size confinement of the metal particles is thus believed to enhance their electrochemical activity towards the formation/decomposition of Li$_2$O.

Choi et al. [14] studied electrochemical insertion-extraction of lithium into CoO with X-ray absorption spectroscopy (XAS) in the first cycle. The formula Li$_y$CoO was proposed. From his study Li$_y$CoO should be seen as the intermediate product when lithium is inserted into CoO.

Based on the results of above ex-situ XRD, EXAFS and SEM studies on the lithiation and delithiation of LaCoO$_3$ as well as the reaction mechanism of cobalt oxide with lithium in Li-ion cells, we propose following mechanism for the reactions of LaCoO$_3$ with lithium in an electrochemical cell:

$$LaCoO_3 + Li \rightarrow \frac{1}{2}Li_2O + \frac{1}{2}La_2O_3 + CoO \quad (1)$$
$$CoO + 2Li \leftrightarrow Co + Li_2O \quad (2)$$
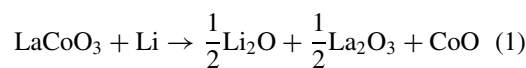
When the cell is discharged, reaction (1) is thermodynamically feasible and thereby expected so that CoO is produced. The lithium insertion is accompanied by the formation of clusters and the decreasing size of the particles. Then reaction (2) is also feasible according to Poizot et al. [3]. Since after reaction (2) the Co nano-particles are dispersed in a lithia (Li_2O) matrix, with the Li_2O + nano-particles being surrounded by a solid electrolyte interface, the reaction (2) can be reversible to some extent so that the $LaCoO_3$ electrode displays a certain reversible capacity. It can be understood that the displacive redox reaction (2) must take place at the interface between the Co particles and the Li_2O "separation layer". During the charge step, the outer portion of the Co particles is oxidized into CoO, forming a CoO(shell)/Co(core) structure. The further oxidation should involve in the diffusion of oxygen from the CoO surface to Co core through the CoO shell. Since the CoO is not a good oxygen conducting material, the rate of this process would be eventually kinetically controlled. The depth of the oxygen diffusion must be dependent on the current density and the size of the core-shell structure. Hence, with the decreasing of the particle size with cell cycling, the electrochemical activity of Li_2O is enhanced.

Reaction (2) may be described as the following two-step reactions according to Choi et al.'s study [14]:

$$CoO + yLi \rightarrow Li_yCoO(0 \leq y \leq 1) \qquad (3)$$

$$Li_yCoO + (2 - y)Li \rightarrow Li_2O + Co \qquad (4)$$
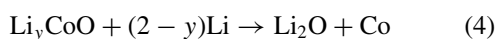
This two-step reaction is consistent with the two reduction/oxidation peaks observed on the CV curves for the subsequent cycles (Fig. 3). A change in the slope on the voltage profile for the second discharge process can be also seen at about 0.8 V (Fig. 4). Nevertheless, this slope change is hardly observed in the subsequent cycles. Based on Choi et al.'s very detailed EXAFS study, the y value is determined to be between 0.78 and 1.32 [14]. However, the exact value seems not match with their electrochemical measurements.

The above reaction mechanism differs from the classical mechanisms, which are based either on reversible insertion/extraction of lithium into host structure or on lithium alloying reactions. This proposed mechanism can interpret the CV curves, the voltage profiles and the irreversible capacity for $LaCoO_3$ electrode. When the coin cell is cycled, in the first discharged process reaction (1) firstly takes place and the particle size

is decreased which accelerates the processing of reaction (2). In the following cycles only reaction (2) is reversible. Therefore, the first discharge process is different from the subsequent discharge process. The large irreversible capacity of the first cycle includes not only the lithium consumed in the formation of SEI film but also the lithium consumed in reaction (1).

If this electrochemical milling process and the core-shell structure are the reason for the reversible reaction, the reversible capacity should be dependent on the crystallinity and microstructure of the initial $LaCoO_3$ material. To study this we compare the cycling results of two cells with $LaCoO_3$ sintered at 900 and 1100°C as the electrodes. As already shown in Fig. 2, the morphology of $LaCoO_3$ sintered at 900°C has a less crystallinity than the $LaCoO_3$ sintered at 1100°C and its particle size is smaller than the 1100°C-sintered $LaCoO_3$. From the capacity data of these two cells (Fig. 5), we can see that the $LaCoO_3$ (900°C) has a higher reversible capacity than $LaCoO_3$ (1100°C). This reflects again that the smaller the core-shell structure is, the greater the reversible capacity can be achieved.

4.   Conclusions

$LaCoO_3$ powders were prepared by a polymerizable complex (PC) route. Its electrochemical performances as a possible electrode material in lithium battery were investigated. After the first discharged process it has a certain reversible capacity. Depending on the sintering temperature, this reversible capacity is about 130 mAh/g for 900°C and 110 mAh/g for 1100°C. From the ex-situ XRD, EXAFS and SEM of lithiated/delithiated $LaCoO_3$ electrode, a reaction mechanism of $LaCoO_3$ with lithium involving the production of La_2O_3 and CoO as the imtermediate products is proposed. Furthermore, we use a CoO(shell)/Co(core) model to explain the reversible capacity as a function of initial $LaCoO_3$ particle size.

National Synchrotron Radiation Laboratory on the EX-AFS analysis.

References

1. Y. Idota, T. Kubota, A. Matsufuji, Y. Maekawa, and T. Miyasaka, *Science*, **276**, 1395 (1997).
2. N.C. Li and C.R. Martin, *J. Electrochem. Soc.*, **148**, 164 (2001).
3. P. Poizot, S. Laruelle, S. Grugeon, L. Dupont, and J.-M. Tarascon, *Nature*, **407**, 496 (2000).
4. G.X. Wang, Y. Chen, K. Konstantinov, M. Lindsay, H.K. Liu, and S.X. Dou, *J. Power Sources*, **109**, 142 (2002).
5. G.X. Wang, Y. Chen, K. Konstantinov, J. Yao, J.H. Ahn, H.K. Liu, and S.X. Dou, *J. Alloys and Compounds*, **340**, L5 (2002).
6. F. Huang, Z.Y. Yuan, H. Zhan, and Y.H. Zhou, *J.T. Sun, Mater. Lett.*, **57**, 3341 (2003).
7. R. Alcantara, M. Jaraba, P. Lavela, and J.L. Tirado, *Chem. Mater.*, **14**, 2847 (2002).
8. N. Sharma, K.M. Shaju, G.V.S. Rao, and B.V.R. Chowdari, *Electrochem. Commun.*, **4**, 947 (2002).
9. C.H. Chen, H. Kruidhof, H.J.M. Bouwmeester, and A.J. Burggraaf, *J. Appl. Electrochem.*, **27**, 71 (1997).
10. C.H. Chen, H.J.M. Bouwmeester, R.H.E. van Doorn, H. Kruidhof, and A.J. Burggraaf, *Solid State Ionics*, **98**, 7 (1997).
11. M. Popa and M. Kakihana, *Solid State Ionics*, **151**, 251 (2002).
12. G. Thornton, B.C. Tofield, and A.W. Hewat, *J. Solid St. Chem.*, **61**, 301 (1986).
13. J.M. Tarascon, A.S. Gozdz, C. Schmutz, F. Shokoohi, and P.C. Warren, *Solid State Ionics*, **86–88**, 49 (1996).
14. H.C. Choi, S.Y. Lee, and S.B. Kim, *J. Phys. Chem. B*, **106**, 9252 (2002).